Memoirs of the Faculty of Engineering, Okayama University, Vol.36, No.1, pp.41-49, December 2001

Structure and Cohesive Energy of Large Spherical Coulomb Clusters

Hiroo TOTSUJI,* Tokunari KISHIMOTO, Chieko TOTSUJI, and Kenji TSURUTA
Department of Electrical and Electronic Engineering, Okayama University
Tsushima-naka, Okayama 700-8530, Japan

(Received November 12, 2001)

The ground state of spherical clusters of charged particles of one species confined by the three-dimensional parabolic potential is investigated by molecular dynamics simulations with the system size from $N = 5000$ to $N = 1.2\times10^5$. The cohesive energy per particle is compared between the shell-structured clusters and spherical finite bcc lattices with relaxed surfaces, the former and the latter being the ground states for small systems and for the large enough systems, respectively. It is shown that, when $N > N_c (N_c > N)$, finite bcc lattices with relaxed surfaces (the shell structures) have stronger cohesion than the shell structures (finite bcc lattices with relaxed surfaces) and the critical value of the transition N_c is estimated to be $10^4 < N_c < 1.4 \times 10^4$. The nucleation of the bcc lattice in the shell-structured cluster of 2×10^4 ions is observed.

I. INTRODUCTION

Large clusters of laser-cooled ions confined in the Penning-Malmberg and the Paul traps have provided us with clear examples of the strongly coupled plasma [1–4]. One of most remarkable phenomena observed there is the crystallization of ions of one species induced by mutual Coulomb interaction. Since the effect of traps is equivalent to the existence of the uniform neutralizing background charges and the bcc lattice is the ground state of the (infinite) one-component plasma (OCP) [5], one may expect to have the bcc lattice at the central part of large enough clusters where the geometry of confinement may not influence the structure significantly.

In experiments, the bcc lattice has been observed at the central part of clusters of the size more than a few times 10^5 [6, 7]: For smaller clusters, shell structures which reflect the geometry of confinement have been observed. Based on the one-dimensional calculations, the transition of the ground state from the shell structure to the bcc lattice in the spherically symmetric system has been estimated to occur at the system size of 10^5 or larger [1]. Though numerical simulations are expected to give more precise information related to this transition and the largest spherical

*totsuji@elec.okayama-u.ac.jp

system reported has 20000 ions [8], extensive analyses have not been performed. The purpose of this paper is to compare the structures and cohesive energies of large clusters of charges with the system size from $N = 5000$ to $N = 1.2 \times 10^5$.

II. COHESIVE ENERGY OF COULOMB CLUSTERS

We consider the one-component plasma confined by the spherically symmetric parabolic potential. The Hamiltonian of our system H is written as $H = K + U$, where U is the potential energy given by

$$U = \sum_{i>j}^{N} \frac{q^2}{|\mathbf{r}_i - \mathbf{r}_j|} + \sum_{i=1}^{N} \frac{1}{2} k \mathbf{r}_i^2 \tag{2.1}$$

and K, the kinetic energy. We define the Wigner-Seitz radius a by $a = (q^2/k)^{1/3}$ and rewrite U into the form

$$U = \left(\frac{q^2}{a}\right) \left(\sum_{i>j}^{N} \frac{1}{|\mathbf{r}'_i - \mathbf{r}'_j|} + \sum_{i=1}^{N} \frac{1}{2} (\mathbf{r}'_i)^2 \right), \tag{2.2}$$

normalizing the coordinates of particles by a.

When charges are regarded as continuum (the fluid approximation), the ground state is the uniform distribution up to the radius $R = (Nq^2/k)^{1/3} = N^{1/3}a$ with the density $n = (3/4\pi)(k/q^2)$. We note that a is the average mean distance or the ion-sphere radius in this approximation; $(4\pi/3)na^3 = 1$. The potential energy of the ground state in the fluid limit U_{homo} is given by $U_{homo} = (9/10)N^{5/3}(q^2/a)$. For given configurations of particles, we define the cohesive energy per particle u_{coh} by $u_{coh} = (U - U_{homo})/N$ and compare u_{coh} for various structures. When the system size is infinite, u_{coh} reduces to the Madelung energy of OCP [5].

At zero temperature, the behavior of the system is determined only by U and (2.2) indicates that our system is characterized by only one parameter, the system size N. At finite temperatures, we define the parameter Γ which represents the strength of the Coulomb coupling by $\Gamma = q^2/k_B T a$. The static properties of the system at finite temperatures are characterized by the parameter Γ and the system size N.

In the fluid approximation, the radius of uniform distribution oscillates with the frequency $\omega_p = (3k/m)^{1/2} = (4\pi q^2 n/m)^{1/2}$. The time $2\pi/\omega_p$ characterizes the macroscopic evolution of our system. One of characteristic time scales of the microscopic evolution may be the time to traverse the mean distance by thermal velocity $a/(k_B T/m)^{1/2} = (3\Gamma)^{1/2}(2\pi/\omega_p)$.

III. MOLECULAR DYNAMICS

We perform the molecular dynamics simulations employing the fast multipole method with the $O(N)$-scaling under controlled accuracy [9]. In this method, the system is divided recursively into small cells and the interaction between particles belonging to well-separated cells is computed based on the multipole expansion and Taylor expansion. The number of smallest cells is 8^{level}

and the level is adjusted so that the smallest cell has about 8 particles on the average. In our simulations for the system size around 10^5, we adopt the level 5, multipole expansion up to 2^6-th order, the Taylor expansion up to 6th order, and the well-separatedness 2 (in the finest division, direct computation is applied for nearest and next-nearest neighbor cells). In the course of molecular dynamics simulation, the accuracy of the cohesive energy is kept at least for the first 4 digits and the direct computation is performed for final relaxed states. The parameters for smaller systems are also determined to give the accuracy at least of the same order. The temperature is controlled by the Nosé-Hoover thermostats [10]. In order to keep the homogeneity of the temperature, we attach multiple thermostats each controlling the kinetic energy of about 5000 particles. We anneal the system for a sufficiently long time or cool the system step by step sufficiently slowly, waiting for the potential and kinetic energies to settle at each specified temperature. The resultant time scale of annealing or cooling is much longer than $2\pi/\omega_p$ and $2\pi(3\Gamma)^{1/2}/\omega_p$.

We start from two kinds of initial conditions; (A) the uniform random distribution of particles within the sphere of the radius R, and (B) the spherical cutout of the bcc lattice (spherical bcc matter). In both cases, initial velocities are given by the random distribution corresponding to the temperature specified by Γ. These two sets of initial conditions lead to different final zero-temperature states when the temperature is slowly lowered. The former gives shell-structured clusters while the latter gives finite bcc lattices with reconstructed surfaces.

A. Shell-Structured Clusters

When we start from the initial condition (A), we first anneal the system at the temperature above the melting point of OCP (with typical values of Γ around 100) and then slowly cool the system. With the decrease of the temperature, the formation of spherical shells advances from the periphery to the center. The system sizes of our simulations are $N = 5000$, 10^4, 20288, and 10^5 and Figs. 1 and 2 show the radial distribution functions and the particle distributions near the equatorial plane in the final state of some examples. Outer shells are clear and well-defined, the radial distribution function hitting zero between them. The sharpness of shells decreases with the decrease of the distance from the center. However, we still have shells near the center though they are diffuse and cannot be decomposed completely.

For a given N, the final configuration depends on the history of cooling and the initial conditions (within (A)). To check this dependency, we have followed two examples for $N = 5000$ and 10^4 and in other cases, repeated annealing and cooling . After sufficiently slow cooling, the radial distribution is very similar especially for the outer part. The cohesive energy is also similar and the difference in the fourth leading digit seems to be less than 2: The cohesion usually becomes stronger by repeated annealing but once cooled down sufficiently slowly, the cohesive energy does not change to such an extent. This may indicate that there exist many local minima of the total potential energy with similar values for the shell-structured configurations.

The values of the cohesive energy of the shell-structured spherical systems are shown in TABLE I and plotted in Fig. 3. These values can be interpolated as

$$\frac{u_{coh}}{q^2/a} = -0.89503 + 0.0401 N^{-1/3} \tag{3.1}$$

for $5000 < N < 10^5$. We note that the cohesive energy of shell-structured states is not expected to have well-defined asymptotic behavior; when $N \to \infty$, shell structures may even lose the stability as a local minima of the total potential energy. For our purpose, it is therefore necessary to have the values of cohesive energy for large clusters instead of extrapolating from those of smaller clusters.

B. Spherical bcc Matter with Relaxed Surface

In the initial state (B), the spherical bcc matter has rather high surface energy [1, 11]. The initial cohesive energy depends on the position of the center of the potential well relative to lattice points. Starting from (B), we anneal the system keeping the temperature near but below the melting point. We then lower the temperature slowly and obtain the finite spherical bcc lattice with reconstructed surface. The system sizes of our simulations are N = 4544, 10464, 20288, 48928, and 120032. An example of the structures is shown in Fig. 4. We observe that the relaxation has occurred only within a few layers at the surface. The cohesive energy of the spherical bcc matter with reconstructed surface is shown in TABLE I and plotted in Fig. 3. The relaxation near the surface largely enhances the cohesion [11]. This has not been expected from the weak cohesion of unrelaxed spherical bcc matter.

When we anneal the spherical bcc matter at higher temperatures, the reconstruction of the surface advances inward further. The resultant cohesion of the system, however, becomes weaker. Thus the final states obtained above are local minima which are reached starting from the spherical bcc matter.

In the limit of very large values of N, the cohesive energy the spherical bcc matter with reconstructed surface may have the form

$$\frac{u_{coh}}{q^2/a} = E_\infty + E_s N^{-1/3}, \tag{3.2}$$

where E_∞ = -0.895929 (the Madelung energy of the bcc lattice) and the second term expresses the effect of the surface. When fitted to this form as shown in Fig. 3 by the solid line, we have $E_s = 0.0598$.

IV. COMPARISON OF COHESIVE ENERGIES AND CRITICAL SYSTEM SIZE

The cohesive energies of the shell-structured clusters and of finite bcc matters with relaxed surface are compared in Fig. 3. We observe that, when the system size exceeds the critical

value N_c, stronger cohesion is given by finite bcc lattices with relaxed surfaces rather than shell-structured clusters. The critical system size is estimated from (3.1) and (3.2) as $N_c = 1.05 \times 10^4$. We here note that these cohesive energy, especially of shell structures, could become lower by annealing the system repeatedly. When we estimate the latter effect by changing the fourth digit of the cohesive energy of shell structures by unity, we have

$$1.1 \times 10^4 < N_c < 1.5 \times 10^4. \tag{4.1}$$

The above critical system size is smaller than the value expected from the experimental observations. In this relation, we note that the shell-structured cluster is still a metastable state at a local minimum of the total potential energy in the domain $N > N_c$ where bcc lattices with relaxed surfaces have lower total potential energies. Therefore it is not strange that the shell-structured clusters with $N > N_c$ do not evolve into bcc lattices with relaxed surfaces in our simulations. The system has to overcome the barrier of the total potential energy in order to relax to lower energy state and, once the system is in the state of higher potential energy, it takes a very long time for the main part of the system to be organized into lattices. In addition to this, clusters of ions are rotating in experiments, and any effects which disturb the solid rotation, such as collisions with residual atoms and molecules, may keep the system from being organized into lattices as a whole. Thus we may regard our critical value not in contradiction with experimental observations.

As discussed above, it is not expected that shell structures go under the structural transition in the process of cooling even when $N > N_c$. One may, however, expect that there is a chance for small bcc lattices to develop in the clusters of larger sizes.

In the distribution of particles shown in Fig. 2, there exists a domain where we have a regular straight structure rather than planes curved in accordance with the surface. The structure factor for 48 particles included in a sphere centered in this domain is shown in Fig. 5. We clearly see that the Bragg spots forms the fcc structure in the wave-number space. We have confirmed that the spacing between Bragg spots is consistent with the bcc lattice with the average density of this cluster within a few percent. This domain thus forms the bcc lattice nucleated from the shell-structured cluster.

To summarize, it is shown that finite bcc lattices with relaxed surfaces have stronger cohesion relative to shell-structured clusters when the system size exceeds about 10^4. In the shell-structured cluster of 2×10^4, the nucleation of the bcc lattice is observed.

TABLE I: Cohesive energy of shell-structured clusters and finite bcc lattices with relaxed surfaces. Figures in ( ) are ambiguity in the fifth digit estimated by two examples.

shell-structured cluster		bcc with relaxed surface	
N	u_{coh}	N	u_{coh}
5000	-0.89268(6)	4544	-0.89232
10000	-0.89315(1)	10464	-0.89335
20288	-0.89359	20288	-0.89375
100000	-0.89415	48928	-0.89410
		120032	-0.89460

Acknowledgments

This work has been partly supported by the Grants-in-Aid for Scientific Researches of the Ministry of Education, Culture, Sports, Science, and Technology, Nos. 08458109 and 11480110.

[1] For a review, D. H. E. Dubin and T. M. O'Neil, Rev. Mod. Phys. **71**, 87 (1999).

[2] S. L. Gilbert, J. J. Bollinger, and D. J. Wineland, Phys. Rev. Lett. **60**, 2022 (1988).

[3] G. Birkl, S. Kassner, and H. Walther, Nature (London) **357**, 310 (1992).

[4] M. Drewsen, C. Broderson, L. Hornekær, J. S. Hangst, and J. P. Schiffer, Phys. Rev. Lett. **81**, 2878 (1998).

[5] S. G. Brush, H. L. Sahlin, and E. Teller, J. Chem. Phys. **45**, 2102(1966).

[6] W. M. Itano, J. J. Bollinger, J. N. Tan, B. Jelenković, X. -P. Huang, and D. J. Wineland, Science **279**, 686 (1998).

[7] J. J. Bollinger, T. B. Mitchell, X. -P. Huang, W. M. Itano, J. N. Tan, B. Jelenković, and D. J. Wineland, Phys. Plasmas, **7**, 7 (2000).

[8] J. P. Schiffer, *Non-Neutral Plasma Physics II*, edited by J. Fajans and D. H. E. Dubin, AIP Conference Proceedings 331, New York, 1995, p. 191.

[9] L. Greengard and V. Rokhlin, J. Comput. Phys. **73**, 325 (1987).

[10] S. Nosé, J. Chem. Phys. **81**, 511(1984).

[11] T. Kishimoto, C. Totsuji, K. Tsuruta, and H. Totsuji, Physics Letters A **281**, 256 (2001).

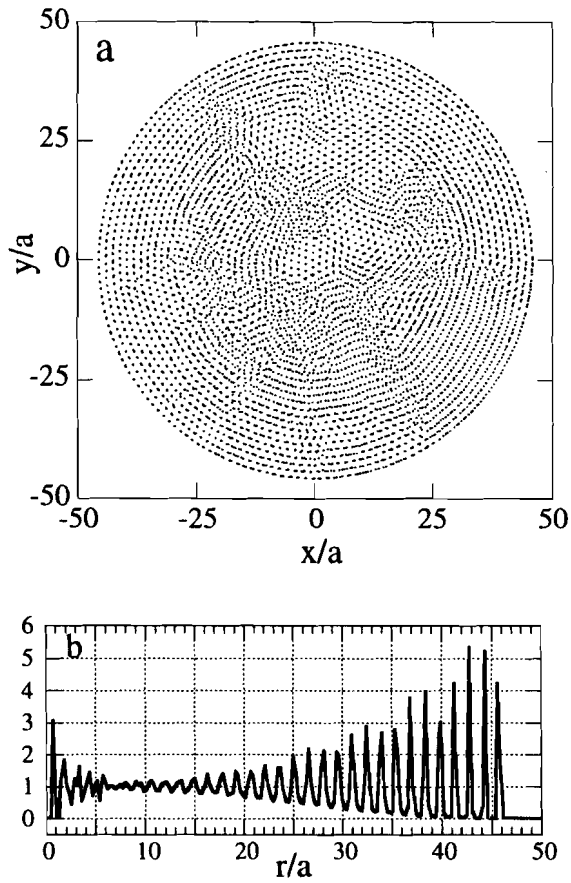

FIG. 1: Shell-structured cluster of 10^5 charges. Configuration near equatorial plane with $|z| < 2.06a$ (a) and radial distribution normalized by average density (b).

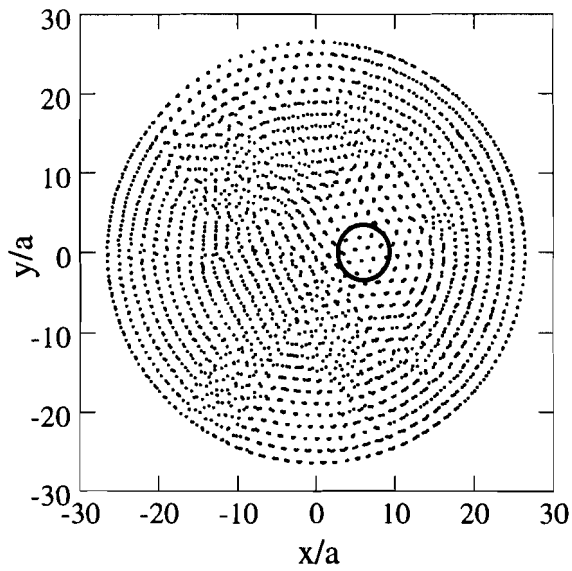

FIG. 2: The same as Fig. 1a for shell-structured cluster of 20288 charges. Configuration is shown for particles with $|z| < 2.42a$.

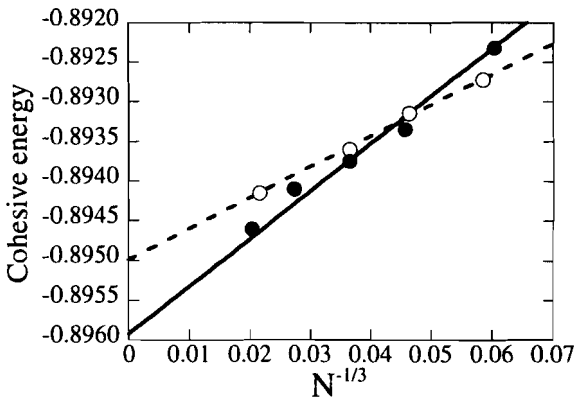

FIG. 3: Cohesive energy per particle of spherical Coulomb clusters. Open and filled circles are shell-structured clusters and finite bcc lattices with relaxed surfaces, respectively, and broken and solid lines are interpolations.

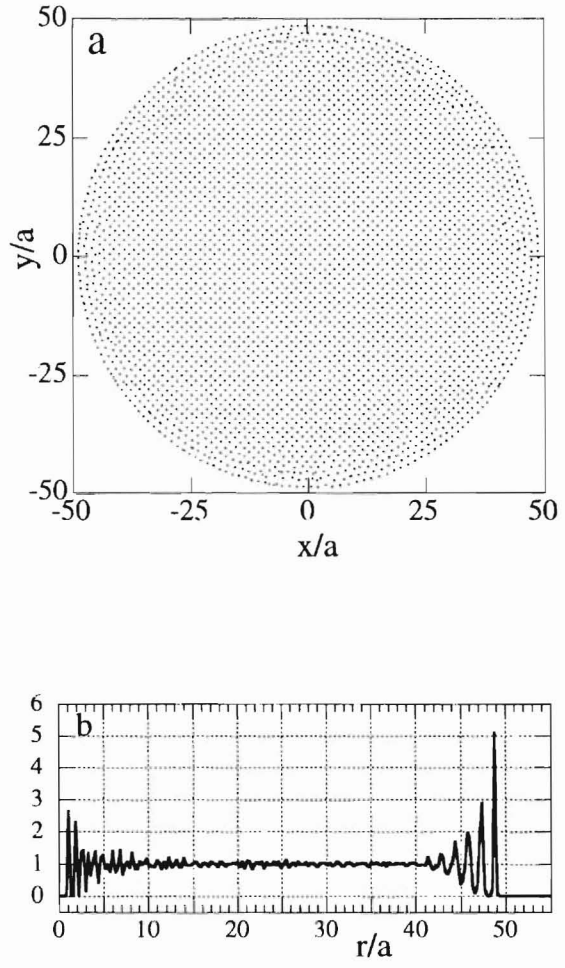

FIG. 4: The same as Fig. 1 for finite bcc lattice of 120032 charges with reconstructed surface. Configuration (a) is shown for particles with $|z| < 2.19a$.

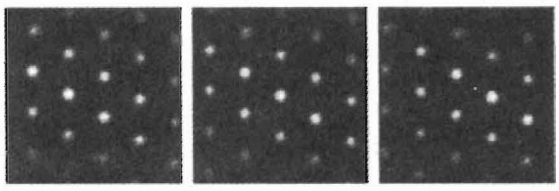

FIG. 5: Bragg patterns from particles in the central part of the shell-structured cluster of 20288 charges: The particles are in a sphere centered at $(6.06, 0, 0)a$ shown by solid line in Fig. 2. These planes, $\mathbf{k} \cdot \mathbf{n}/(2\pi/a) = -0.569, 0, 0.569$ (from left to right), $\mathbf{n} = (-0.0764, -0.0643, 0.995)$, form three successive close packed (111) planes in the fcc lattice.